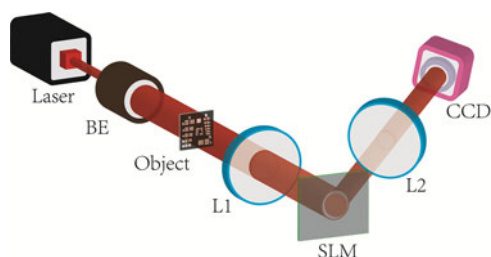# Super-Resolution Imaging Using Compressive Sensing and Binary Pure-Phase Annular Filter

Yicheng Sun
Guohua Gu
Xiubao Sui
Yuqi Li
Shuangshuang Xu

IEEE

Super-Resolution Imaging Using Compressive Sensing and Binary Pure-Phase Annular Filter

Yicheng Sun,[1,2] **Guohua Gu,**[1] **Xiubao Sui,**[1] **Yuqi Li,**[2]
and Shuangshuang Xu[3]

[1]School of Electronic and Optical Engineering, Nanjing University of Science and Technology, Nanjing 210094, China
[2]NRIEE, Nanjing 210007, China
[3]CEC Panda LCD Technology Co., Ltd., Nanjing 210000, China

Abstract: Super-resolution is an important goal for the diffraction-limited optical system. In this paper, we present a novel technique that exceeds the limit of resolving power of the diffraction-limited optical system to achieve super-resolution imaging by combining compressive sensing with a binary pure-phase annular filter. This novel technique is achieved by using a classical 4F optical system with a pure-phase spatial light modulator. The feasibility of this imaging technique is theoretically analyzed and physically validated by laboratory experiments.

Index Terms: Superresolution, optical system, phase-only filters.

1. Introduction

The limit of resolving power of optical systems set by diffraction was, for the case of coherent illumination, first described by Abbe [1]. The more exact formulation of the diffraction limitation is that an optical system transfers a limited band of spatial frequencies, due to the numerical aperture (NA) and the optical wavelength.

Super-resolution (SR) imaging techniques, such as grating techniques and annular filters, aim at overcoming the diffraction limitation by generating synthetic aperture or reducing the central spot size of the point-spread function (PSF) [2]–[8]. Although grating techniques can dramatically expand the cutoff frequency of an optical system, the payment is to reduce the field of view (FOV) around the region of interest (ROI), and precision gratings with a high basis frequency are also required. Annular filters are well-known methods in the optical shaping, such as design of optical needle, optical tweezers and so on [6]–[8]. They try to narrow the main lobe of PSF, and lead to a reduction of the spot size with respect to the diffraction limitation embodied in the Airy disk pattern. However, the number of samples captured by using these two techniques should be enough to guarantee the reconstruction quality of the high-resolution (HR) object. This will raise an additional budget for a large plane array charges coupled device of an image acquisition system.
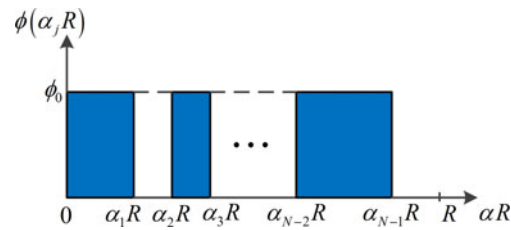
Fig. 1. Phase value of each zone of the BPAF.

Along with the presentation of compressive sensing (CS), signals occupying a very large bandwidth but with a sparse spectrum can be reconstructed from a small amount of measurements [9], [10]. Consequently, CS has been well applied in the field of compressive imaging, by utilizing the fact that the information in natural images is redundant [11]—[13]. The main motivation of this work is to propose a novel SR imaging technique, which combines CS with a binary pure-phase annular filter (BPAF). In this novel technique, CS allows the reconstruction of HR object's image from a small number of captured samples by utilizing the fact that natural images are sparse in arbitrary representation basis. BPAF allows the resolution improvement of the optical system beyond the diffraction limit. To the best of our knowledge, and after searching the literature, this is the first work to demonstrate the feasibility of this SR imaging technique. This technique also uses a single exposure acquisition process without requiring any other measurement dimensions, and any movement against to some conventional SR imaging systems.

This paper is organized as follows: In Section 2, we simply introduce the theoretical background of BPAF. In Section 3, we discuss the feasibility of our SR technique. In Section 4, we provide experimental results. We conclude the paper in Section 5.

2. Theoretical Background of BPAF

According to the diffraction theory, for a circular aperture, the shape of PSF of a point is an Airy disk. An annular filter is a kind of rotationally symmetric diffractive super-resolution elements relative to the circular aperture. Let us consider a complex pupil function $P(\alpha_j R) = T(\alpha_j R) \exp[i\phi(\alpha_j R)]$ of an annular filter, where R is the radius of the circular aperture, $\alpha_j R$ defines the radial position of each zone, and α_j defines normalized boundary coordinate with $\alpha_0 = 0$ and $\alpha_N = 1$, by definition. $T(\alpha_j R)$ is the amplitude function, and $\phi(\alpha_j R)$ is the phase function. $\phi(\alpha_j R) =$ constant produces amplitude-only annular filters while $T(\alpha_j R) =$ constant generates phase-only annular filters. BPAF is a class of phase-only annular filters. In the BPAF case, each element of $T(\alpha_j R)$ is equal to one, and each element of each zone of $\phi(\alpha_j R)$ can assume only two possible values illustrated in Fig. 1.

In order to design the optimized radius and phase value of each zone of the BPAF, we need to consider three very important parameters: Strehl ratio S, normalized spot size G, and side lobe intensity I_R. Lower G, I_R and higher S values are expected for the design of the BPAF. Normally, an increase of resolution (the decrease of G) is accompanied by a decrease of S, which reflects the increase of I_R by several orders of magnitude with respect to the central core. As a result, the usable FOV can be dramatically reduced. According to Reference [4], if I_R is less than 0.1, the FOV influenced by the side lobe intensity will be still acceptable. Furthermore, for a given normalized spot size, there is an upper bound on the value of the Strehl ratio for any degree of resolution [5].

Consequently, we firstly specify the value of G, and then utilize the optimization method to solve the maximum problem of S with some constraints:

$$\max S, \ s.t \begin{cases} G = c\,[c \text{ is constant}], \ I_R \le 0.1 \\ T(\alpha_j R) \in [0, 1], \ \phi(\alpha_j R) \in 0 \text{ or } 0.8\pi. \end{cases} \tag{1}$$
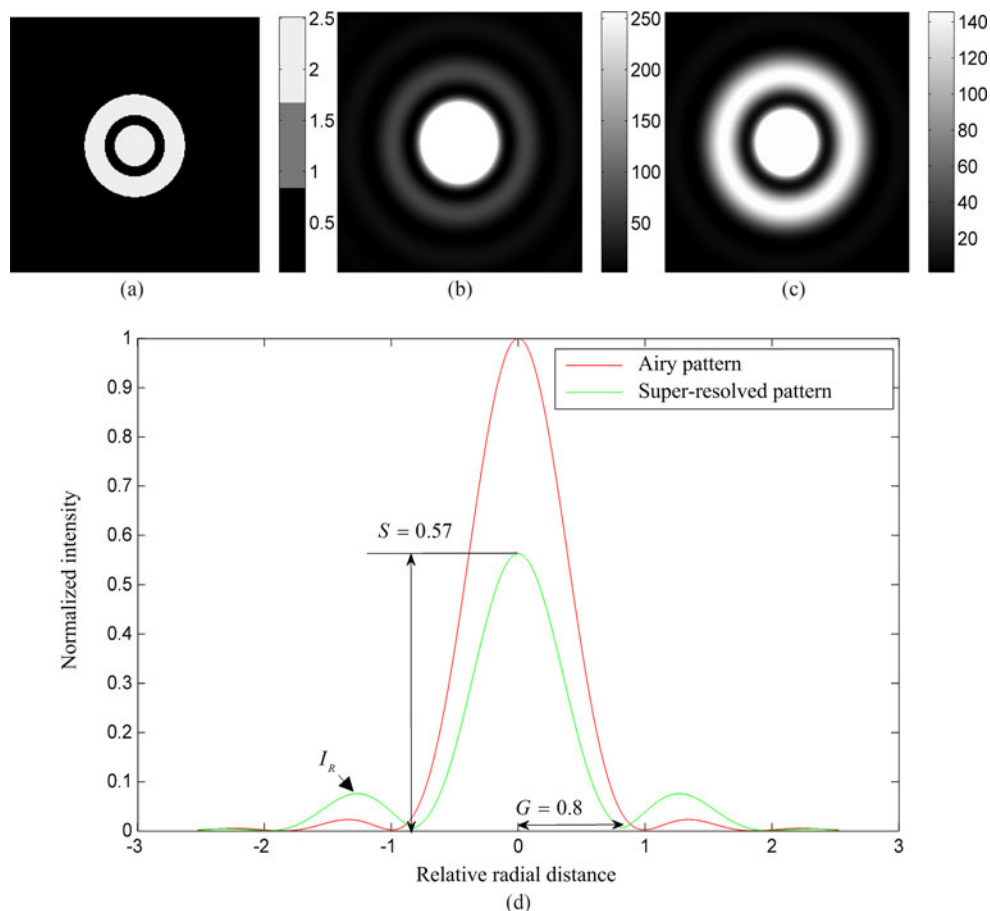
Fig. 2. Simulation results. (a) Designed BPAF. (b) Airy disk pattern. (c) Super-resolved pattern. (d) Normalized intensity distribution curve.

Equation (1) is performed by using the nonlinear programming method of MATLAB's constrained optimization toolbox, and the constrained nonlinear function **fmincon()** is chosen to suit our design. For a given $G = 0.8$, we designed a BPAF with four zones. The simulation results are presented in Fig. 2. Fig. 2(a) shows the designed BPAF with radii $(0, 0.16, 0.24, 0.4, 1)$ and phase value $(0.8\pi, 0, 0.8\pi, 0)$. The Airy disk pattern and the super-resolved pattern obtained by using the designed BPAF are presented in Fig. 2(b) and (c), respectively. Fig. 2(d) shows the slice normalized intensity distribution curve produced by the super-resolved pattern (green curve) and the Airy disk pattern (red curve). We can find that G and S are 0.8 and 0.57, respectively. Moreover, I_R is less than 0.1. According to [6], the theoretical resolution improvement factor for the diffraction-limited optical system caused by the designed BPAF is approximate to 1.245.

3. Super-Resolution Imaging Using CS and BPAF

The schematic diagram of the system for the proposed SR imaging technique is presented in Fig. 3. The setup is a classical 4F optical system, where λ is the wavelength of the spatially coherent light, z_f is the focal length of Fourier lenses L_1 and L_2. Assuming that an achievable two-dimensional (2-D) HR object has a size of n pixels, and a complex-field distribution $f_h(u, v)$. The complex-field distribution $K(\xi, \eta)$ of the detector plane can be expressed as an inverse Fourier transform of the
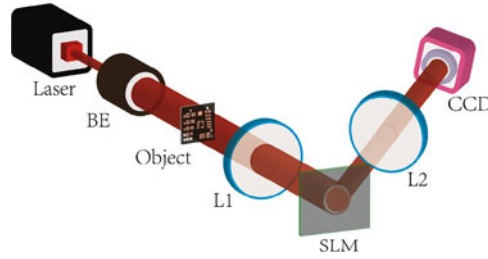
Fig. 3. Schematic diagram: BE, beam expender; L1, L2, Fourier lens; SLM, spatial light modulator; CCD, charged-coupled device.

phase modulated spectrum:

$$K(\xi, \eta) = \iint F_h(x, y) \times circ(\sqrt{x^2 + y^2}/R) \times \exp[i\phi(\alpha_i R)]$$

$$\times \exp\left[-i\frac{2\pi}{\lambda z_f}(\xi x + \eta y)\right] dx dy. \tag{2}$$

$F_h(x, y)$ is expressed as the Fourier transform of $f_h(u, v)$:

$$F_h(x, y) = \iint f_h(u, v) \times \exp\left[-i\frac{2\pi}{\lambda z_f}(ux + vy)\right] du dv. \tag{3}$$

$circ(\sqrt{x^2 + y^2}/R)$ is the pupil function of the circular aperture, and $\exp[i\phi(\alpha_i R)]$ is the exponential phase modulation term produced by the designed BPAF.

Substituting (3) into (2), we can obtain the relationship between $f_h(u, v)$ and $K(\xi, \eta)$. For mathematical simplicity, the matrix formulation of this relationship can be written as

$$K = \Im^{-1}w\Im f_h \, , \, f_h = \Psi s, \tag{4}$$

where f_h and K are the column vectorized versions of $f_h(u, v)$ and $K(\xi, \eta)$ in lexicographic ordering, respectively. $\Im$ denotes the 2-D discrete Fourier transform matrix with a size of $n \times n$, $\Im^{-1}$ is the inverse Fourier transform of $\Im$, w denotes the diagonal matrix with a size of $n \times n$ whose diagonal non-zero entries are $circ(\sqrt{x^2 + y^2}/R) \times \exp[i\phi(\alpha_i R)]$, Ψ is an orthogonal sparse basis, and s is the sparse coefficient matrix of f_h in Ψ.

Observing the right side of (4), we find that the term of $\Im^{-1}w\Im$ can be rewritten as a circulant matrix C with a size of $n \times n$. The first row entries c_{1j} of C are the inverse Fourier transform of the diagonal elements of w. According to the RIPless theory, if the Fourier components of entries in C have the same magnitude, the circulant matrix C is an isometry, and obeys a simple incoherence property and an isotropy property [14]. After sampling K at randomly selected locations, one can faithfully recover the approximately sparse coefficient matrix of f_h from a minimum number of noisy measurements [14]. Consequently, for a stable reconstruction, the number of measurements m required for the RIPless theory should satisfy

$$m \geq u(C) \times k_s \log^2 n. \tag{5}$$

$u(C)$ denotes the coherence parameter of C, and is defined by $u(C) = \max |c_{ij}|^2$. k_s is the number of non-zero entries of the sparse coefficient matrix. The intensity distribution I_R after random sampling can be written as

$$I_R \cong D_R \odot |K|^2 + \varepsilon_{ccd}$$

$$= D_R \odot \left|\Im^{-1}w\Im f_h\right|^2 + \varepsilon_{ccd} = D_R \odot |Cf_h|^2 + \varepsilon_{ccd} \tag{6}$$

where D_R is a sampling mask which obeys with 0 and 1 random distribution, and randomly selects m measurements. According to mathematical knowledge, (6) can be rewritten as

$$I_R = D_R \odot |Cf_h|^2 + \varepsilon_{ccd} = |D_R \odot Cf_h|^2 + \varepsilon_{ccd} \qquad (7)$$

where $\odot$ denotes the Hadamard product operation, and ε_{ccd} denotes the random noise.

The recovery of complex-field distribution K_R of measurements can be accomplished by using an iterative phase-retrieval algorithm with some support constraints, e.g., the modulus of K_R is nonnegative and equal to the measured modulus $\sqrt{I_R}$, and the sampling extent of CCD is at least equal to that of the auto-correlation of the object's size [15]—[17]. Once K_R is recovered, f_h can be reconstructed by solving the following minimization problem:

$$\hat{s} = \underset{s}{\operatorname{argmin}} \frac{1}{2} \|K_R - D_R \odot Cf_h\|_2^2 + TV_\gamma(f_h) \qquad (8)$$

where $\hat{s}$ is the optimal solution, and $TV(\cdot)$ stands for the discrete total variation (TV) regularization term. The reconstructed complex-field distribution $f_h{}'$ can be estimated by $f_h{}' = \Psi\hat{s}$. In this work, we focus more on the intensity distribution $I_h{}' = f_h^{*\prime}f_h{}'$, where $f_h^{*\prime}$ is the complex conjugate of $f_h{}'$.

4. Experimental Results

The experimental setup of the proposed SR imaging technique is presented in Fig. 4(a). For the spatially coherent monochromatic illumination, the setup consisted of a He-Ne laser beam at a wavelength of 632.8 nm (Thorlabs HNL020R), a $\times$ 10 objective lens (Thorlabs RMS10X), and a single-mode optic fiber (Daheng Optics XSM-FC/PC). The object was a USAF target (Thorlabs R3L3S1N). The 4F optical system contained two lenses (Thorlabs LA1708) with a focal length 200 mm and a diameter 25.4 mm, and a SLM (Cambridge SDE1024) with 1024 $\times$ 768 pixels and a pixel pitch of 9 μm. A CCD (Pioneer Times PNT-698) with 720 $\times$ 576 pixels and a pixel pitch of 9 μm was placed on the output focal plane of the 4F system to capture intensity images. Consequently, the sampling cutoff frequency of the CCD caused by geometric limitation was approximately 55.6 lp/mm.

A circular aperture with a radius of 2.304 mm was attached to the front plane of the display window of SLM, therefore, the coherent cutoff frequency of the 4F optical system was $F_{off} = R \lambda z_f = 18.20$ lp/mm. Since the sampling cutoff frequency was much larger than the coherent cutoff frequency, the geometric resolution limitation caused by the shape and pitch of the pixel in the CCD was neglected in our experiment. According to the coherent cutoff frequency, the elements of Group 4-7 in the USAF target were chosen as the illuminated object, and the other elements were blocked. The size of the illuminated object was pre-set to 1.4 mm $\times$ 1.6 mm. Since the amplification factor of the 4F system is 1, the pixel pitch of the illuminated object is also 9 μm. In order to facilitate the calculation, the size of reconstructed images of the object is pre-determined by 256 $\times$ 256 pixels. To obtain a high diffraction efficiency and achieve the spatial isolation of signal from noise in the first diffracted order, we first used the encoding method proposed in Reference [18] to generate the phase modulation about the designed BPAF, and secondly added the phase modulation to a 1-D pure-phase grating with a basic frequency of 18.20 lp/mm. The finally generated phase modulation pattern with 256 gray-level is presented in Fig 4(b). Two random sampling masks whose number of 1 respectively accounted for 25% and 50% of the total number of reconstructed SR images are presented in Fig. 4(c) and (d). Consequently, the sampling ratio of two masks was 0.25 and 0.5, respectively. The relaxed averaged alternating reflections (RAAR) algorithm and the two-step iterative shrinkage/thresholding (TwIST) algorithm were used to reconstruct K_R and $f_h{}'$, respectively [19], [20].

The experimental results are presented in Fig. 5. Fig. 5(a) is the low resolution (LR) image captured with the circular aperture, and without the designed BPAF. According to the diffraction theory, the frequencies of the elements in Fig. 5(a) beyond the coherent cutoff frequency cannot pass through the optical system, therefore they are all blurred. Fig. 5(b) and (c) are the reconstructed SR results by using the proposed technique from the aforementioned two random sampling masks,
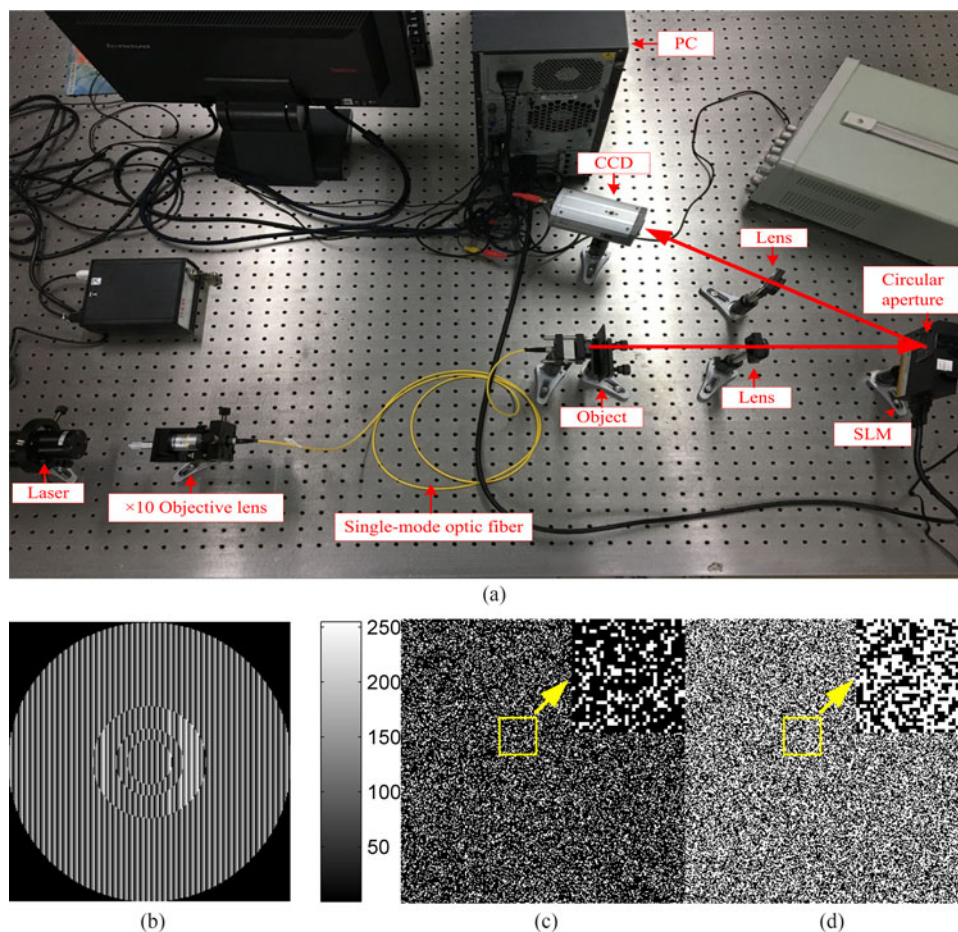
Fig. 4. (a) Experimental setup. (b) Phase modulation pattern. (c), (d) Random sampling mask with 0.25 and 0.5 sampling ratios, respectively.

respectively. Fig. 5(d) is the HR reference image of the illuminated object captured without the circular aperture. According to the Nyquist-Shannon criterion, the highest spatial resolution in Fig. 5(d) is limited by the sampling cutoff frequency of the CCD. Fig. 5(e)–(h) are $\times 2.8$ zooms of the red regions in Fig. 5(a)–(d), respectively. Due to the coherent cutoff frequency, the observably element of the USAF in Fig. 5(a) is Group 4 Element 2, whose spatial resolution is less than 18.20 l p/mm. The approximately observably element of the USAF in Fig. 5(b) is Group 4 Element 4, whose spatial resolution can be computed by the following formula:

$$\text{Resolution } (lp/mm) = 2^{Group + (Element-1)/6}. \tag{9}$$

According to (9), the highest spatial resolution in Fig. 5(b) improved by our technique is 22.63 l p/mm. The ratio of the highest frequency 22.63 l p/mm and the cutoff frequency 18.20 l p/mm is 1.243, and demonstrates that the practical resolution improvement factor is close to the theoretical value.

Next, we used the aforementioned experimental device to provide comparative experiments for Chan's technique [12], Romberg's technique [13], and our technique. The reason why we chose these two methods is that their methods not only can be easily achieved by the aforementioned experimental setup without the need for additional hardware system, but also are common and effective ones in two fields of both compressive imaging and super-resolution imaging. We still
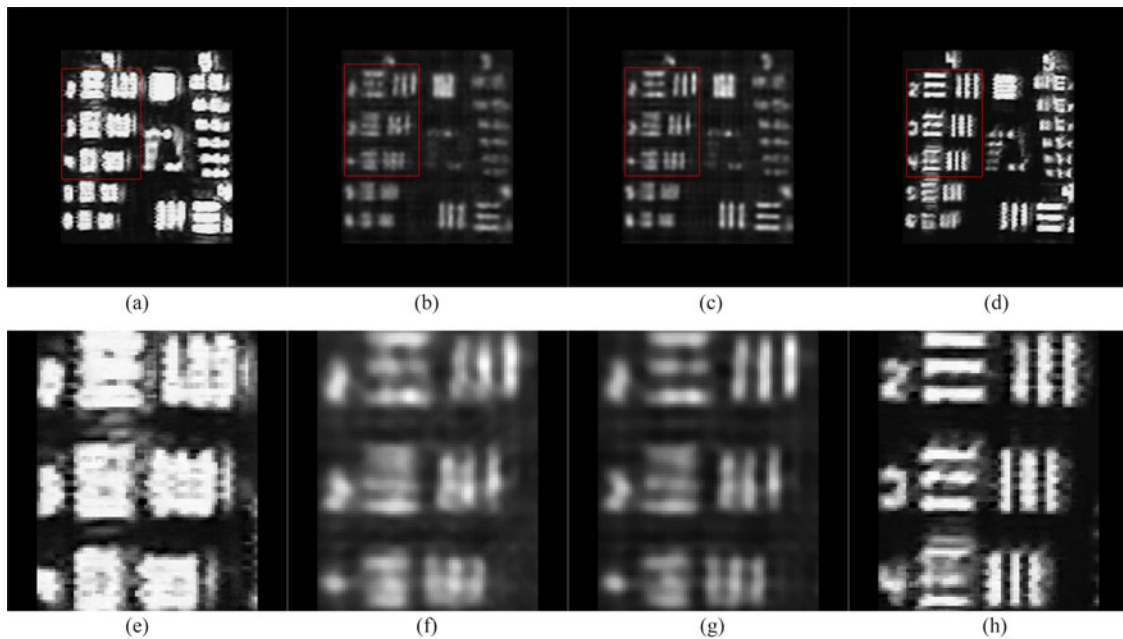
Fig. 5. Experimental results. (a) LR image. (b), (c) Reconstructed SR results from two masks, respectively. (d) HR image. (e)–(h) ×2.8 zooms of red regions in (a)–(h), respectively.
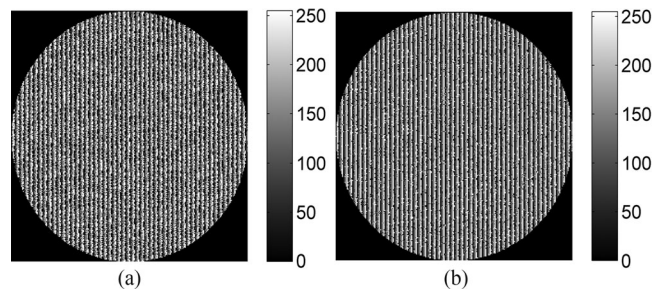

Fig. 6. (a) Phase modulation patterns of Chan's technique [12]. (b) Phase modulation patterns of Romberg's technique [13].

used the encoding method and the pure-phase grating superimposing technique to generate the phase modulation patterns of Chan's technique [12] and Romberg's technique [13]. The patterns are presented in Fig. 6(a) and (b), respectively.

At this time, the mask with 0.25 sampling ratio was chosen for comparative experiments. Moreover, Fig. 5(d) was utilized as the calculational reference, which objectively assessed the quality of reconstructed results. We loaded different phase modulation patterns to obtain the measurements of different techniques, and used the RAAR and TwIST algorithms to achieve SR reconstruction.

The numerical results of Peak Signal to Noise Ratio (PSNR) and Structural Similarity Index (SSIM) are summarized in Table 1, and the reconstructed SR results are presented in Fig. 7. Fig. 7(a)–(c) are reconstructed SR images by using Chan's technique [12], Romberg's technique [13], and our technique, respectively. Fig. 7(d)–(f) are ×4 zooms of the red regions in Fig. 7(a)–(c), respectively. From Table 1 and Fig. 7, we find that the reconstructed SR result by using our technique is most similar to the HR reference one, and has the observably highest spatial resolution. This is because the BPAF can pull the high-frequency component into the imaging system. In summary, experimental results validate the feasibility of our SR imaging technique.

TABLE 1

PSNR and SSIM Comparisons

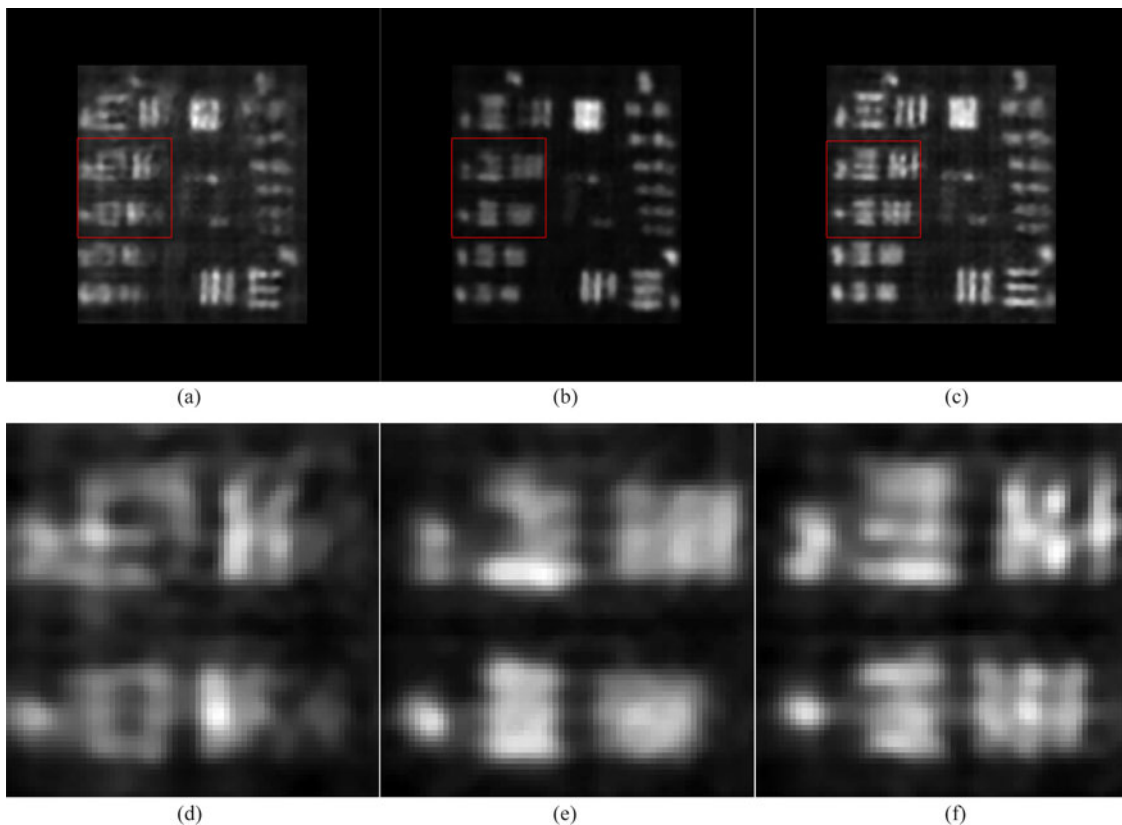|	Chan's technique [12]	Romberg's technique [13]	Our technique
PSNR	11.46	12.02	13.50
SSIM	0.2687	0.3640	0.4326

Fig. 7. Comparative experimental results. (a)–(c) Reconstructed SR results by using Chan's technique [12], Romberg's technique [16], and our technique. (d)–(f) ×4 zooms of red regions in (a)–(c), respectively.

5. Summary

In this paper, a novel SR imaging technique based on CS and BPAF was proposed. The proposed technique is analytically presented, and laboratory experimented for the spatially coherent monochromatic illumination. However, the designed BPAF provides a small resolution improvement factor. This is because there are checks and balances among the Strehl ratio, the normalized spot size and the side lobe intensity. The limitation of our technique is that a large decrease of the normalized spot size is accompanied by a sharp increase of the side lobe intensity, resulting in a rapid reduction of FOV and an unsatisfactory SR reconstruction. Nevertheless, the proposed technique can be used for LR target detection, optical information compression, static scene SR imaging, and video reconstruction.

References

[1] E. Abbe, "Beiträge zur theorie des mikroskops und der mikroskopichen wahrnehmung," *Archiv für mikroskopische Anatomie*, vol. 9, no. 1, pp. 413–418, 1873.

[2] J. Garcia, V. Micó, D. Cojoc, and Z. Zalevsky, "Full field of view super-resolution imaging based on two static grating s and white light illumination," *Appl. Opt.*, vol. 47, no. 17, pp. 3080–3087, 2008.

[3] A. Ilovitsh, V. Mico, and Z. Zalevsky, "Super resolved optical system for objects with finite sizes using circular gratings," *Opt. Exp.*, vol. 23, no. 18, pp. 23667–23679, 2015.

[4] T. R. M. Sales and G. M. Morris, "Diffractive superresolution elements," *J. Opt. Soc. Amer. A*, vol. 14, no. 7, pp. 1637–1646, 1997.

[5] N. A. Ochoa and C. P. Santos, "Super-resolution with complex masks using a phase-only LCD," *Opt. Lett.*, vol. 38, no. 24, pp. 5389–5398, 2013.

[6] D. Juana, V. Canales, P. Valle, and M. Cagigal, "Focusing properties of annular binary phase filters," *Opt. Commun.*, vol. 229, no. 1/6, pp. 71–77, 2004.

[7] H. Wang, L. Shi, B. Lukyanchuk, C. Sheppard, and C. Chong, "Creation of a needle of longitudinally polarized light in vacuum using binary optics," *Nat. Photon.*, vol. 2, no. 8, pp. 501–505, 2008.

[8] K. Huang, P. Shi, X. Kang, X. Zhang, and Y. Li, "Design of DOE for generating a needle of a strong longitudinally polarized field," *Opt. Lett.*, vol. 35, no. 7, pp. 965–967, 2010.

[9] Y. Sun, G. Gu, X. Sui, Y. Liu, and C. Yang, "Single image super-resolution using compressive sensing with a redundant dictionary," *IEEE Photon. J.*, vol. 7, no. 2, Apr. 2015, Art. no. 6900411.

[10] D. Donoho, "Compressed Sensing," *IEEE Trans. Inf. Theory*, vol. 52, no. 4, pp. 1289–1306, Apr. 2006.

[11] V. Farber, Y. August, and A. Stern, "Super-resolution compressive imaging with anamorphic optics," *Opt. Exp.*, vol. 21, no. 22, pp. 25851–25863, 2013.

[12] W. L. Chan, K. Charan, D. Takhar, K. Kelly, R. G. Baraniuk, and D. M. Mittleman, "A single-pixel terahertz imaging system based on compressed sensing," *Appl. Phys. Lett.*, vol. 93, no. 12, pp. 121105–121109, 2008.

[13] J. Romberg, "Compressive sensing by random convolution," *SIAM. J. Imag. Sci.*, vol. 2, no. 4, pp. 1098–1128, 2009.

[14] E. Candes and Y. Plan, "A probabilistic and RIPless theory of compressed sensing," *IEEE Trans. Inf. Theory*, vol. 57, no. 11, pp. 7235–7254, Nov. 2011.

[15] J. R. Fienup, "Reconstruction of an object from the modulus of its Fourier transform," *Opt. Lett.*, vol. 3, no. 1, pp. 27–29, 1978.

[16] R. Horisaki, Y. Ogura, M. Aino, and J. Tanida, "Single-shot phase imaging with a coded aperture," *Opt. Lett.*, vol. 39, no. 22, pp. 6466–6469, 2014.

[17] Y. Xu, L. Du, Q. Li, and H. Qin, "Passive forensic technology for digital image," *Command Inf. Syst. Technol.*, vol. 7, no. 1, pp. 7–12, 2016.

[18] J. A. Davis, D. D. Cottrel, J. Campos, M. J. Yzuel, and I. Moreno, "Encoding amplitude information onto phase-only filters," *Appl. Opt.*, vol. 38, no. 23, pp. 5004–5013, 1999.

[19] D. R. Luke, "Relaxed averaged alternating reflections for diffraction imaging," *Inverse Problems*, vol. 21, no. 1, pp. 37–50, 2005.

[20] J. M. Bioucas and M. A. T. Figueiredo, "A new TwIST: Two-step iterative shrinkage/thresholding algorithms for image restoration," *IEEE Trans. Image Process.*, vol. 16, no. 12, pp. 2992–3004, Dec. 2007.